Inorganic Chemistry

Article

pubs.acs.org/IC

Structural Modulation and Phase Transitions in $La_2CoO_{4.14}$ Investigated by Synchrotron X-ray and Neutron Single-Crystal Diffraction

Loïc Le Dréau,[†,‡] Carmelo Prestipino,*[,†] Olivier Hernandez,[†] Jürg Schefer,[‡] Gavin Vaughan,[§] Serge Paofai,[†] Juan Manuel Perez-Mato,[∥] Shoichi Hosoya,[⊥] and Werner Paulus*[,⊗]

[†]Institut des Sciences Chimiques de Rennes, Université de Rennes 1, UMR CNRS-UR1 6226, Campus de Beaulieu, Bât 10B, 35042 Rennes Cedex, France

[‡]Laboratory for Neutron Scattering, Paul Scherrer Institute, CH-5232 Villigen PSI, Switzerland

[§]European Synchrotron Radiation Facility, ID11, Grenoble, France

[∥]Departamento de Fisica de la Materia Condensada, Facultad de Ciencias, Universidad del Pais Vasco, UPV/EHU Apdo. 664, E-48080 Bilbao, Spain

[⊥]Institute of Inorganic Synthesis, Faculty of Engineering, Yamanashi University, Miyamae-cho 7, Kofu 400, Japan

[⊗]Institut Charles Gerhardt, Université de Montpellier, UMR 5253 CNRS-ENSCM-UM2-UM1, 8 rue de l'Ecole Normale, 34296 Montpellier, France

Supporting Information

ABSTRACT: We report a combined synchrotron X-ray and neutron diffraction study on as-grown $La_2CoO_{4.14}$ single-crystal from 10 to 470 K. Unprecedented structural features in terms of a (3 + 2)D incommensurate modulation have been detected and characterized in the Low Temperature Orthorhombic (LTO) phase already at room temperature despite the complex twinning that was unravelled. A new intermediate phase between the LTO and High Temperature Tetragonal (HTT) phases has been observed for the first time (in the range of 413−433 K). The transformation from LTO to this so-called HTLO (High Temperature Less Orthorhombic) phase is associated to a lowering of orthorhombicity and a loss of one modulation vector, yielding a (3 + 1)D incommensurate modulation. Conversely, above 433 K the HTT phase appears as nonmodulated but exhibits a strong dynamic disorder of CoO_6 octahedra, which has been characterized in detail by reconstruction of nuclear densities via the Maximum Entropy Method (MEM).

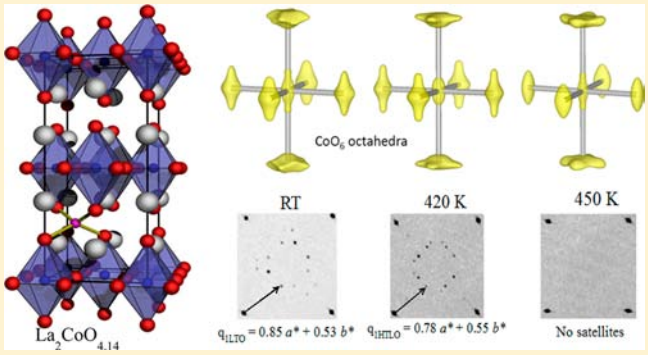

INTRODUCTION

The Ruddlesden−Popper phases of general formula $A_{n+1}B_nO_{3n+1}$ have been extensively studied for their electronic, structural and chemical properties and especially the case $n = 1$, that is, the K_2NiF_4 structure-type, since the discovery of high T_C superconducting properties in $(La, Ba)_2CuO_4$ system.[1] Hole creation in La_2MO_4 (M = Co, Ni, Cu) series can be achieved either by partial substitution of La with alkaline cations ($La_{2-x}R_xMO_4$) or by intercalation of overstoichiometric oxygen anions on interstitial lattice sites ($La_2MO_{4+\delta}$).[2,3] The effects of cation-doping on the physical properties of this family of oxides have been well described after several years of intense studies, while the oxygen diffusion process remains not fully understood although electrochemical oxidation occurs already at ambient temperature for those compounds.[4−6] However, this feature is a clue for the fundamental understanding of low-temperature oxygen diffusion mechanism in solid oxides with respect to their potential technological applications (e.g., oxygen separation membrane in SOFCs, oxygen sensors, and so forth). Reducing the operating temperature of such devices would avoid the problems linked to the thermal stability of the materials. The stoichiometric $La_2CoO_{4.0}$ oxide appears to be the best candidate in the course of exploring oxygen diffusion at moderate temperature for its surprising chemical reactivity. Indeed, it has been shown to be subject of spontaneous oxidation under atmospheric conditions from $\delta = 0$ to 0.16;[7] this has never been observed neither on the cuprate nor on the nickelate.

Only few studies are reported about $La_2CoO_{4+\delta}$ although it owns the advantage to exhibit a high intercalation rate up to $\delta = 0.25$ corresponding to one extra oxygen per F unit cell as shown

Received: June 1, 2012
Published: September 5, 2012

   dx.doi.org/10.1021/ic301165a | Inorg. Chem. 2012, 51, 9789−9798

in Figure 1 (δ_{max} goes from 0.07 to 0.12 for $La_2CuO_{4+\delta}$[8] and from 0.18 to 0.25 for $La_2NiO_{4+\delta}$[9,10]). The high stability of III

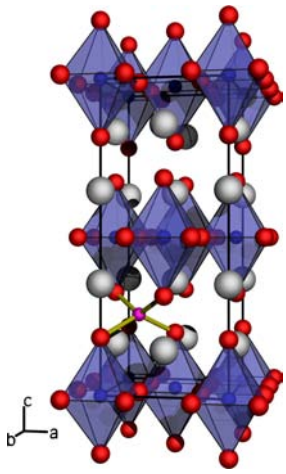

Figure 1. *F*-centered average unit cell, no distortion of octahedra has been represented. Cobalt, Lantanum and oxygen atoms are represented in blue, white, and red, respectively. The interstitial oxygen site is represented in magenta, and its coordination with yellow sticks.

valence state of cobalt encourages the oxidation by turning metastable Co^{2+} ions into Co^{3+} when O^{2-} is inserted in the lattice (up to 50% Co^{2+} and 50% Co^{3+} for δ_{max} = 0.25). Contrary to the Cu and Ni compounds, the *c*-axis parameter of the cobaltate astonishingly decreases for high δ values. The $La_2CoO_{4+\delta}$ compound has been found to undergo several structural phase transitions between orthorhombic and tetragonal states versus δ and *T*.[2,11,12] However the structural complexity for high δ values was not detected or was not properly understood. The main difficulties in describing precisely the atomic structure when $\delta \neq 0$ are coming from the partial occupation of tetrahedral interstitial sites ($^1/_4$ $^1/_4$ $^1/_4$, 8*i*) of the orthorhombic *F* unit cell by extra oxygen atoms that modify their local environment by steric effect. The interstitial oxygen O_{int} atoms are located between CoO_6 octahedra layers and possess four apical oxygen atoms (O_{ap}) in their first coordination sphere. The O_{ap} are consequently shifted from their basic positions because of their repulsive interaction with O_{int}, forcing their corresponding CoO_6 octahedra to tilt around some specific directions of the *a*-*b* plane (depending on δ and *T*) to open the tetrahedral site for O_{int}. Thus, the structural modifications caused by the intercalation consist in both, a partial occupation of interstitial sites (occ_{max} = 1/8 for δ = 0.25) and a distortion of the octahedra arrangement. The basic structure of oxygen-rich compounds is modulated by shifts of the positions of O_{ap} that are correlated to the occupancy of O_{int}. This causes a loss of three-dimensional (3D) ordering of CoO_6 tiltings which is equivalent to a stacking disorder of adjacent CoO_6 layers.[13] Consequently, the symmetry space group of the basic unit cell changes from *Bmab* to an average symmetry *Fmmm* (disappearance of the $k + l = 2n + 1$ reflection) when interstitial sites are partially occupied.[14] However, the extra oxygen atoms are not necessarily randomly distributed in the crystal lattice, but may exhibit long-range orders. Consequently, superlattice reflections may arise with $\delta > 0$, up to high $\sin\Theta/\lambda$ values.[14] The complete depiction of the real atomic structure of $La_2CoO_{4+\delta}$ necessitates the use of new models with superspace symmetries that undergo transitions as function of δ and *T*. However, on the practical side, studies are limited by the availability of good quality single-crystal samples and by twinning effects.

The exploration of the structural phase diagram of $La_2CoO_{4+\delta}$ would obviously enhance the comprehension of the oxygen diffusion mechanism by providing the knowledge of the precise oxygen positions and displacements versus *T* and δ. Unfortunately, the structural modulation has never been thoroughly investigated for the oxygen-rich $La_2CoO_{4+\delta}$, only a magnetic modulation at low *T* has been reported until now.[12] A propagation vector has been used for the description of the antiferromagnetic ordering due to a Co^{2+} spin flip occurring below 80 K where the structure undergoes a first-order phase transition to a magnetic tetragonal unit cell of same dimensions but with a different symmetry (space group *P*42/*ncm*) reported by Yamada et al.[11] Nevertheless, in view of the results presented hereafter, the structural modulation related to oxygen intercalation remains much more complex since it implies atomic displacements that must not be neglected in the structural depiction of those technologically and fundamentally important materials.

The previous studies of phase transitions between room temperature (RT) and high temperatures in $La_2CoO_{4+\delta}$ have been exclusively focused on the Low Temperature Orthorhombic (LTO)/High Temperature Tetragonal (HTT) transition,[2,12] ignoring completely superlattice reflections. Here we report a detailed study of the single-crystal structure evolution of $La_2CoO_{4.14}$ *as grown* compound in a range of temperature for which the oxygen content δ remains unchanged (from RT to 500 K). Reciprocal space map reconstructions from hard synchrotron X-ray single-crystal diffraction experiments permitted to follow the evolution of the structural modulation by visualizing superlattice reflections. In complement, the maximum entropy method applied to neutron single-crystal diffraction data sets, collected for different specific temperatures, allowed to single out the contribution of oxygen to the average structure and to reconstruct the 3D nuclear density isosurfaces in the average unit cell, providing a direct view of the structural features. These coupled structural investigations enabled distinguishing a new intermediate stable phase emerging in a narrow range of temperature between LTO and HTT phase due to the presence of interstitial oxygen atoms. Indeed, two reversible phase transitions have been detected: (i) at 410 K from LTO to a High Temperature Less Orthorhombic (HTLO) phase accompanied by a clear variation of the incommensurate modulation (ii) at 430 K the transition from HTLO phase to HTT with a total disappearance of the superlattice reflections.

EXPERIMENTAL SECTION

Sample Synthesis. $La_2CoO_{4.14}$ single-crystals were grown in a lamp-image floating zone furnace at about 1900 K under controlled argon atmosphere. Initial $La_2CoO_{4+\delta}$ powders were prepared by a solid-state ceramic route. High purity La_2O_3 and Co_3O_4 starting reactants were supplied by Aldrich with a purity of 99.99% (Alpha Aesar, Ward Hill, MA, U.S.A.) and 99.98%, respectively (Aldrich Chemical Co., Milwaukee, WI, U.S.A.).[12] La_2O_3 was calcined at 900 °C for 12 h prior to the synthesis to decompose eventual traces of lanthanum hydroxide. After mixing in appropriate ratio, powders were pressed into pellets and sintered at 1200 °C for 24 h under argon flux, this process being repeated three times. The obtained product has been characterized by X-ray powder diffraction (Bruker AXS D8 Advance, LynxEye detector) confirming the high purity of the samples. The powders have then been pressed hydrostatically into Ø6 × 10 cm

dx.doi.org/10.1021/ic301165a | *Inorg. Chem.* 2012, 51, 9789−9798

Table 1[a]

atom	x/a	y/b	z/c	occ	U11	U22	U33	U12	Ueq
				T = 10 K[b]					
La	0	0	0.361(2)	2	0.010(8)	0.010(8)	0.002(7)		0.008(1)
Co	0	0	0	1	0.008(1)	0.008(1)	0.006(8)		0.007(3)
Oeq	1/4	1/4	0	2	0.011(5)	0.011(5)	0.030(8)	0.001(1)	0.017(9)
Oap (1)	0	0	0.173(4)	1.41(2)	0.025(5)	0.025(5)	0.003(5)		0.018(1)
Oap (2)	0.07(1)	0.07(1)	0.18(6)	0.58(1)	0.035(5)				0.035(5)
Oint	1/4	1/4	1/4	014(5)	0.032(1)	0.032(1)	0.001(2)		0.002(1)
				T = 373[c] K					
La	0	0	0.360(9)	2	0.015(8)	0.015(8)	0.008(1)		0.013(3)
Co	0	0	0	1	0.011(1)	0.011(1)	0.022(3)		0.014(7)
Oeq	1/4	1/4	0	2	0.014(9)	0.014(9)	0.031(5)	0.001(3)	0.020(4)
Oap (1)	0	0	0.173(3)	1.65(1)	0.040(3)	0.040(3)	0.015(6)		0.032(1)
Oap (2)	0.09(5)	0.09(5)	0.18(3)	0.36(1)	0.03(7)				0.03(7)
Oint	1/4	1/4	1/4	0.14(1)	0.041(5)	0.041(5)	0.01(6)		0.033(1)
				T = 420[d] K					
La	0	0	0.360(6)	2	0.014(3)	0.014(3)	0.007(1)		0.011(9)
Co	0	0	0	1	0.008(1)	0.008(1)	0.035(8)		0.017(3)
Oeq	1/4	1/4	0	2	0.015(4)	0.015(4)	0.029(2)	0.002(4)	0.020(2)
Oap (1)	0	0	0.174(2)	1.59(1)	0.044(1)	0.044(1)	0.009(6)		0.032(6)
Oap (2)	0.08(9)	0.08(9)	0.17(6)	0.34(7)	0.036(4)				0.036(4)
Oint	1/4	1/4	1/4	0.14(2)	0.009(2)	0.009(2)	0.01(6)		0.011(4)
				T = 450 K[e]					
La	0	0	0.360(9)	2	0.010(6)	0.010(6)	0.004(1)		0.008(4)
Co	0	0	0	1	0.005(4)	0.005(4)	0.014(6)		0.008(5)
Oeq	1/4	1/4	0	2	0.009(9)	0.009(9)	0.032(5)	0.002(3)	0.017(4)
Oap (1)	0	0	0.174(5)	1.37(6)	0.031(6)	0.031(6)	0.002(8)		0.021(6)
Oap (2)	0.07(5)	0.07(5)	0.17(8)	0.54(4)	0.034(5)				0.034(5)
Oint	1/4	1/4	1/4	0.14(4)	0.007(2)	0.007(2)	0.003(8)		0.006(1)

[a] n = occupation probability per formula unit. Atomic displacement factor for O_{ap} (2) have been refined using isotropic coefficients. $U_{13} = U_{23} = 0$ for all atoms. Data collected with TriCS, 4-circle single crystal neutron diffractometer (PSI, SINQ spallation source, Villigen Switzerland), wavelength of neutrons: 1.178(1) Å. Refinements carried out with *JANA2006*. [b] $a = b = 5.48(7)$ Å and $c = 12.62(5)$ Å, $\alpha = \beta = \gamma = 90°$. $V = 380.1(1)$ Å^3, $2\Delta = 1.21°$. Average structure refined in $F4/mmm$ on 112 independent main reflections. $R_{int} = 3.6\%$. Agreement factors on LS refinements: $R = 3.41\%$, $R_w = 3.86\%$. [c] $a = b = 5.50(2)$ Å and $c = 12.642(4)$ Å, $\alpha = \beta = \gamma = 90°$. $V = 382.7(1)$ Å^3, $2\Delta = 1.13°$. Average structure refined in $F4/mmm$ on 112 independent main reflections. $R_{int} = 3.9\%$. Agreement factors on LS refinements: $R = 3.26\%$, $R_w = 4.22\%$. [d] $a = b = 5.50(5)$ Å and $c = 12.675(4)$ Å, $\alpha = \beta = \gamma = 90°$. $V = 384.1(1)$ Å^3, $2\Delta = 0.33°$. Average structure refined in $F4/mmm$ on 112 independent main reflections. $R_{int} = 3.1\%$. Agreement factors on LS refinements: $R = 3.76\%$, $R_w = 4.14\%$. [e] $a = b = 5.510(1)$ Å and $c = 12.697(3)$ Å, $\alpha = \beta = \gamma = 90°$. $V = 385.4(9)$ Å^3, $2\Delta = 0°$. Space group $F4/mmm$, 112 independent main reflections. $R_{int} = 4.2\%$. Agreement factors on LS refinements: $R = 3.93\%$, $R_w = 3.72\%$.

rods. The lower rod corresponding to the seed was purely stoichiometric La_2CoO_4, while the nutritient rod was enriched by an overstoichiometric amount of CoO of 3% molar to compensate the loss of cobalt that evaporates from the substance during growth (testified by a deposition of CoO inside the quartz tube container after the synthesis).

The system $La_2CoO_{4+\delta}$ melts incongruently. The presence of a solvent (CoO) in the molten zone is mandatory. Thus, the synthesis of single-crystals could only be achieved through using the so-called Traveling Solvent Floating Zone technique (TSFZ).[15,16] A supplementary thin rod (3 mm) made of La_2CoO_4 + CoO (50% molar) has been placed at the interface of the seed and nutritient rods to start the growth directly from the proper concentrations of each component. The strong cobalt oxide evaporation has been reduced as much as possible by sharpening the focusing of light using two ad hoc designed halogen lamps (600 W each) equipped with low-size filaments allowing steepening the temperature gradient around the molten zone to maintain the stoichiometry of the nutritient rod as stable as possible before it enters the molten part.[15] The rod so grown has been slowly cooled down to RT manually lowering the power supplied to the lamps during 10 h, approximating a ramp of 2.6 °C/min. Although the precaution taken, the synthesis is very delicate as it is constantly perturbed by the small fluctuations of the growth conditions; therefore, the final crystallized product was not fully homogeneous, and only few crystal pieces (∼1 cm) could be extracted. Each piece has been checked and oriented with a X-ray Laue diffractometer (λ = 1.54056 Å, Photonic Science) revealing the good quality of the samples as well as their homogeneity. Moreover, single-crystal X-ray diffraction measurements (λ = 0.71073 Å, Nonius KappaCCD) performed on different samples (∼100 μm) taken out from each piece permitted to check the crystallinity and the reproducible lattice parameters $a = 5.523(2)$, $b = 5.488(3)$, and $c = 12.645(4)$ Å. The oxygen stoichiometry $La_2CoO_{4.14}$ was determined by thermogravimetric measurements in mixed gas atmosphere flux of 5% H_2/He on a ground portion of the crystal used for neutron experiment. During the measurement, temperature was increased from RT to 1273 K with a heating rate of 10 K/min. The reduction process occurred in the range between 534 and 750 K, and the resulting weight of the decomposed sample remained constant for the rest of the measurement. The total loss of weight, attributed to the oxygen departure, was measured to be 3.97(1) % of the starting sample mass, corresponding to $\delta = 0.14 \pm 0.02$ according the following chemical reaction:

$$La_2CoO_{4+\delta} + H_2 \rightarrow La_2O_3 + Co_{(metal)} + (1 + \delta)H_2O\uparrow$$

The value of $\delta = 0.14$ corresponds to the more stable phase in mild oxidation condition;[2] this stoichiometry is not surprising because although the growth is done in Argon flux the molten zone is over stoichiometric in oxygen.

dx.doi.org/10.1021/ic301165a | Inorg. Chem. 2012, 51, 9789−9798

Supplementary thermogravimetric studies in air have been performed with a NETZSCH Jupiter STA 449C thermobalance coupled with a PFEIFFER Thermostar mass spectrometer on ground *as grown* crystal, showing constancy of oxygen content in the range RT < T < 480 K, followed by mass changing in the range 480 K < T < 800 K (visible in the Supporting Information, Figure S1). In this paper we focus our results only on the temperature range where δ is constant, that is, below 480 K; the upper range of temperature will be the object of a further publication.

Characterization Methods. Single-Crystal Synchrotron X-ray Diffraction. Small sample pieces (∼100 μm) have been followed in situ as a function of temperature by synchrotron X-ray diffraction, on ID11 Materials Science Beamline at ESRF, (Grenoble, France) equipped with a low-noise FReLoN CCD camera.[17] The wavelength has been set to λ = 0.2072 Å, that is, below the K absorption edge of Lanthanum to avoid absorption corrections that are problematic for twinned crystals. To obtain satisfactory separation of the main reflections that are split by the twinning effects and to optimize the detection of superlattice reflections, we decided to favor the angular resolution of the setup, applying a sample/detector distance of 230 mm. The diffraction data have been measured by φ-scans (280° with a step of 0.2°) acquiring 5 images per second, always at constant temperature. The temperature of the sample was controlled by a heat blower. Data integration and pixel by pixel reciprocal plane reconstructions were performed via CrysAlis software (Oxford Diffraction). Structural refinements against diffraction data have been carried out through JANA2006.[18]

Single-Crystal Neutron Diffraction. Neutron diffraction experiments have been performed with the 4-circle diffractometer TriCS[19] at the Swiss spallation source SINQ of the Paul Scherrer Institute (PSI, Villigen, Switzerland). The diffractometer was equipped with a point-detector (He^3-tube) and the wavelength of the thermal neutron beam was set to λ = 1.178(1) Å. A large *as grown* crystal sample (3 × 3 × 5 mm^3) was placed inside a cryofurnace. Few main reflections, as well as satellites, have been scanned continuously in the range of 10 K−470 K, and full data sets have been collected at 10, 300, 420, and 450 K. The structural models have been refined with JANA2006.[18] Nuclear densities have been reconstructed in real space through the Maximum Entropy Method (MEM) via PRIMA[20] (PRactice Iterative Mem Analysis), a program from the package VENUS[21] (Visualization of Electron/NUclear densities and Structures), and the corresponding graphical representations of the results have been obtained thanks to VESTA software[22] (Visualization for Electronic and STructural Analysis).

RESULTS

Synchrotron X-ray Diffraction. Two successive phase transitions have been observed: the first at 413 K, where the orthorhombicity strongly decreases, followed by a second one at 433 K, where a transition from an orthorhombic to a tetragonal unit cell has been clearly observed. The apparent space group deduced against the main reflections remains *Fmmm* for the first two phases, that is, below 433 K, and becomes *F*4/*mmm* above this temperature. At RT, the basic unit cell parameters were refined to a = 5.473(3), b = 5.527(2), and c = 12.642(4) Å. The first phase transition is accompanied by a sudden decrease of orthorhombicity to a = 5.497(2), b = 5.513(3), and c = 12.675(4) Å, finally above 433 K the unit cell becomes tetragonal with a = b = 5.510(1), and c = 12.697(3) Å (see Table 1). For each acquisition, after refining the unit cell and the orientation matrix, a complete set of (hkl) reciprocal planes has been reconstructed pixel by pixel. Below 433 K, the family of planes perpendicular to a* or b* (e.g., ($0kl$) and ($h0l$) planes) show only the expected reflections indexed in accordance with the previously reported structure with the *Fmmm* space group.[39] However, more or less structured diffuse streaks have been observed along c* essentially between specific Bragg reflections, mostly (h06) and (h08). Those lines of diffuse intensity are present for all temperatures but with a slight tendency to be less structured in the HTT phase (see Supporting Information, Figure S2−S4).

Conversely, the planes perpendicular to c*, that is, in the a*-b* plane, exhibit a much more complex arrangement in terms of Bragg spots. Figure 2 shows the ($hk1$) reciprocal space plane

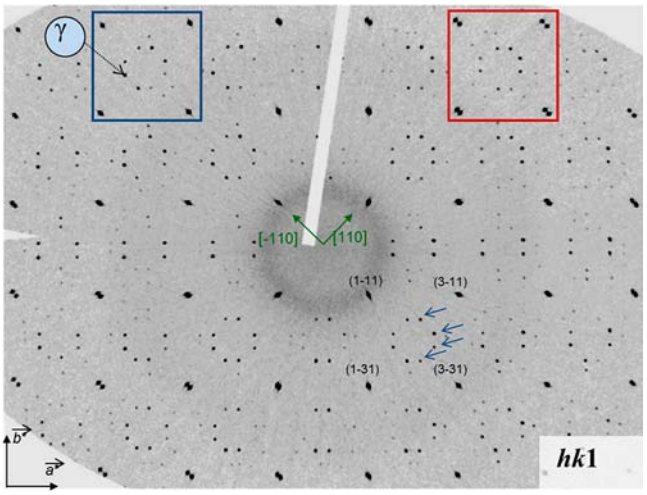

Figure 2. (hk1) reciprocal space plane of $La_2CoO_{4.14}$ at RT (LTO phase), reconstructed pixel by pixel from synchrotron X-ray diffraction data (ID11@ESRF) collected with a CCD detector (FReLoN). Some superlattice reflections are indicated by a blue arrow, one of the more intense satellites corresponding to the 1st order reflections is marked as γ. Red and blue squares underline respectively the splitted region along the [110] direction (green arrow) and the single peaks region along [-110] direction (green arrow).

of *as-grown* $La_2CoO_{4.14}$ at RT, representative of this family of planes for l integer. The reciprocal pattern can be separated into two sets of reflections: spots with high intensity indexed in the *F*-centered unit cell, that is, main reflections, and spots with lower intensity not indexed in the *F*-centered unit cell, that is, satellites (a few of them are indicated by blue arrows in Figure 2). The main reflections lying in the [110] direction are split at high angles (e.g., in the red square in Figure 2), whereas the ones along the [-110] direction remain single peaks (e.g., in the blue square). The splitting of Bragg reflections is due to the presence of two pseudomerohedrally twinned domains with a volume fraction of approximately 60%−40%. This twinning of pseudomerohedral type ensues from the cooling process adopted during the synthesis when the oxides undergo a phase transition from the HTT to the LTO phase triggered by a cooperative tilt of the MO_6 octahedra.[23] The two domains in the sample are differently oriented in the a-b plane, but they share a common c-axis; they are also symmetrical about the (-110) mirror plane of the original HTT cell. Consequently the (-hhl) reflections of domain I are superimposed with the (h-hl) reflections of domain II while the others reflections are partially or fully split depending on 2θ and indexes, as schematized in Figure 3a. It is worth stressing that the presence of only two twin domains is quite rare for the K_2NiF_4 type structure; it is more common to find two sets of two twinned orientations, that is, four domains.[24]

The attribution of satellites to their corresponding domain is not straightforward because of the twinning effect which multiplies the number of satellites. However, thanks to the

dx.doi.org/10.1021/ic301165a | Inorg. Chem. 2012, 51, 9789−9798

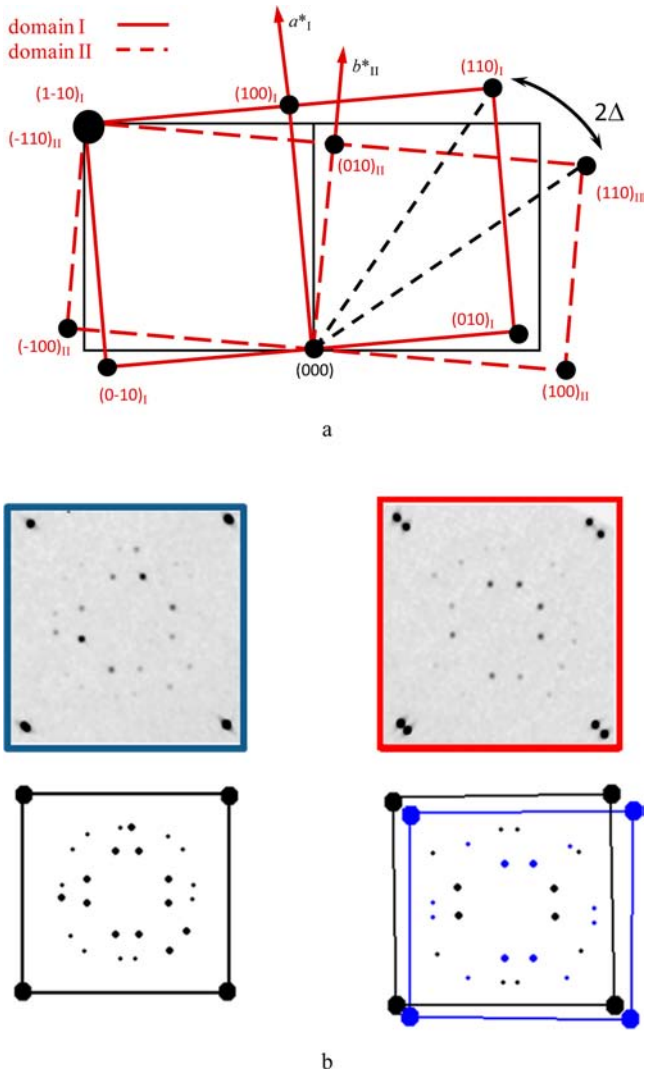

Figure 3. Part (a) shows the twinning law for two domains: the average tetragonal cell (black curve), and the two twin orthorhombic domains (solid and dashed red curves). Part (b) shows a detailed view of red and blue squares of Figure 2 and their respective idealized scheme.

knowledge of the twin law, each satellite can be attributed to its respective domain. This is possible by comparing the pattern in the [110] direction (red square) and the one in the [-110] direction (blue square) corresponding to the right and the left side of Figure 3b. Since satellites are generated by the propagation vector from main reflections, the split induced by twinning causes a related deformation of the satellites' pattern.

Once satellites are ascribed to the first or second domain, all reflections in the ($hk1$) plane can be indexed as shown in Figure 4, where the idealized case of a single domain is presented. For each domain, two symmetric incommensurate propagation vectors are sufficient to index all satellite reflections: $q_{1LTO} = 0.85a^* + 0.53b^*$ (blue) and $q_{1LTO}' = 0.85a^* - 0.53b^*$ (red).

The appearance of up to third order satellites testifies that the modulation corresponding to q_{1LTO} is not purely sinusoidal. On Figure 4, the more intense satellites (one of them marked as γ in Figure 2) correspond to the first order reflections (big full circle) while the others correspond to second order (empty circles) and third order (small full circles). However, the systematic absence of the sum of vector q_{1LTO} and vector q_{1LTO}' (marked x in the Figure 4) suggests that the modulation waves do not coexist in the same structure, but that each pseudomerohedral domain exhibits an additional twinning giving rise to two directions of the modulation vector. Thus, in Figure 4, the blue and red reflections belong to two different domains. The twinning class is of partial merohedral type: main reflections are perfectly overlapped but satellites are systematically separated. Therefore, this second kind of twinning is only observable through satellites, but not via main reflections as they are exactly superimposed. The twin element is the mirror plane perpendicular to b^*, that is, this symmetry element is lost in the average structure and is applied between the twin lattices. As a consequence, although the effect is below the detection limit for basic reflections, the loss of that mirror plane lowers the basic space group to monoclinic $F2/m$.

Figure 5 shows the ($hk^1/_2$) reciprocal space plane of $La_2CoO_{4.14}$ at RT, representative of this family of planes with $l = n + {}^1/_2$. Fundamental reflection are forbidden in this plane, as a consequence all peaks have to be considered as satellites. Upon assigning each peak to domain I or II, it is possible to draw an idealized reciprocal plane ($hk^1/_2$) as shown in Figure 6. To index both types of satellites, for the (hkl) planes with $l = n$ and for $l = n + {}^1/_2$, the use of only one vector is impossible, a second modulation vector is thus mandatory. In the ($hk^1/_2$) plane the more intense reflections (marked β in Figure 5, full circle in Figure 6) are indexed as shown in Figure 6 by the use of a second couple of modulation vectors, with three

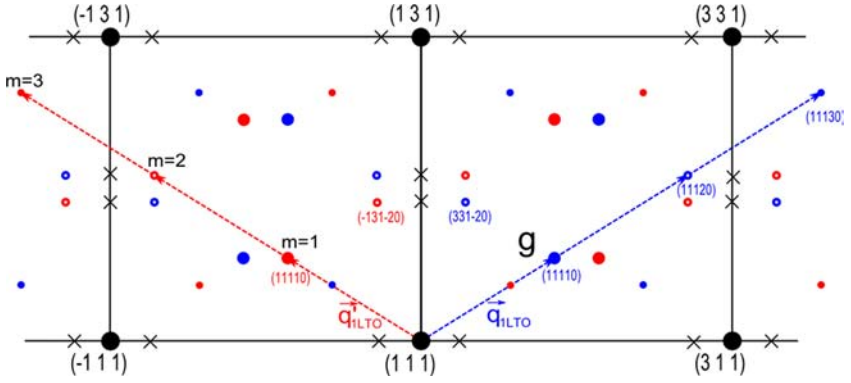

Figure 4. Idealized ($hk1$) reciprocal space plane for a single twinned domain. Blue and red spots refer to the two domains generated by the modulation. Black crosses represent systematic absence of the sum $q_{1LTO} + q_{1LTO}'$.

dx.doi.org/10.1021/ic301165a | Inorg. Chem. 2012, 51, 9789–9798

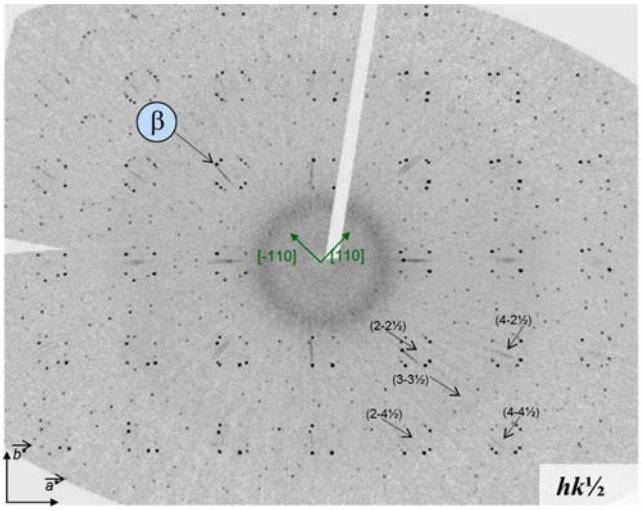

Figure 5. (hk$^1/_2$) reciprocal space plane of $La_2CoO_{4.14}$ at RT (LTO phase), reconstructed pixel by pixel from X-ray synchrotron diffraction data. All the reflections correspond to satellites peaks, the peak corresponding to (*hkl*01) reflection is marked as *β*.

components this time: $q_{2LTO} = -0.23a^* + 0.27b^* + {}^1/_2c^*$ (red full arrow) and $q_{2LTO}' = 0.23a^* + 0.27b^* + {}^1/_2c^*$ (blue full arrow) and correspond to only first order satellites. The systematic absence of the sum $q_{2LTO} + q_{1LTO}'$ and $q_{2LTO}' + q_{1LTO}$ (marked as x in Figure 6) confirms the previous interpretation: the presence of two twins by partial merohedry for each pseudomerohedral domain.

As a conclusion, the investigated crystal at RT is composed of four distinct twin individuals with volumetric repartition of 39−30−21−10% (according to the ratios of equivalent satellites intensities) and for each one all reflections of the full reciprocal lattice, main and satellite, can be indexed with a general reciprocal vector $H = ha^* + kb^* + lc^* + mq_{1LTO} + nq_{2LTO}$ with $0 \leq |m| \leq 3$ and $0 \leq |n| \leq 1$. The angle between the two vectors q_{1LTO} and q_{2LTO} is significantly different from 90°.

Figure 7 shows the temperature dependence of satellites' positions in the region where main reflections are overlapped (red square in Figure 2) for RT, 420 and 450 K. The top part of the figure shows the three experimental patterns whereas the bottom part shows their respective idealized representation for a single domain pattern. The phase stable above 413 K still presents satellite reflections, but the propagation vectors q_{1LTO} shifts to $q_{1HTLO} = 0.783a^* + 0.55b^*$, accompanied by a decrease

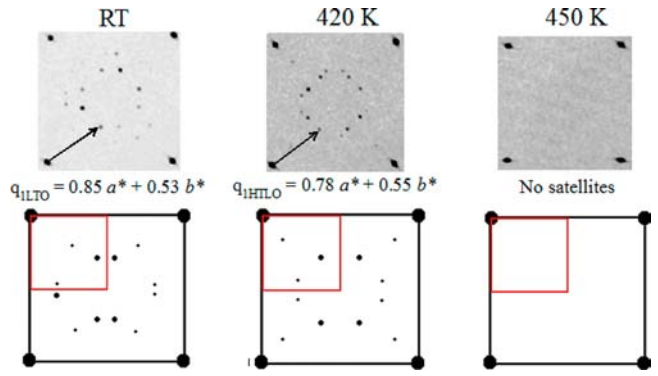

Figure 7. (*hk*1) Reciprocal space plane reconstructed for different temperatures. Variation of the in-plane incommensurate propagation vector is observable at 420 K just before the transition to the HTT phase. The idealized pattern for a single pseudomerohedral twin domain is shown below the experimental patterns.

of orthorhombicity (see Table 1). Moreover the vector q_{2LTO} disappears since the superlattice reflections in the reciprocal planes perpendicular to c^* with $l = n + {}^1/_2$ (n integer) are no longer present. Consequently, at 420 K the indexing of all reflections can be done by using a single modulation vector q_{1HTLO} lying in the *a*-*b* plane for each single domain, with a reciprocal vector $H = ha^* + kb^* + lc^* + mq_{1HTLO}$. This HTLO intermediate phase exhibits an in-plane (3 + 1)D incommensurately modulated structure. Also for this phase the loss of the mirror plane perpendicular to b^* (the twin element) lowers the basic space group to monoclinic *F*2/*m*, in accordance with the condition of admissibility of incommensurate wave vectors that forbid a modulation vector with two incommensurate components for an orthorhombic crystal system.

At 433 K all satellite peaks vanish and the phase becomes nonmodulated and tetragonal as testified by the disappearance of twinning. The reciprocal maps reconstructed for this temperature consists only of *F*4/*mmm* main reflections. Both effects are reversible, satellites reappear with the same propagation vector upon cooling, although the number and the ratio of twinned domains can change as function of the thermal history of the sample.

Because of the specific complex twinning effect of the investigated crystal, it is extremely difficult to obtain accurate integrated intensities of main and satellites peaks for only one domain. Therefore, no refinement of the modulated structure has been attempted. Clearly, structural refinements with a

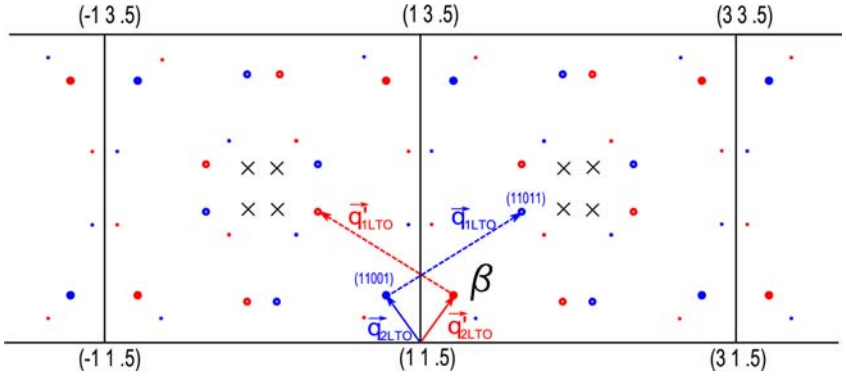

Figure 6. Idealized (*hk*0.5) reciprocal space plane in the LTO phase. Blue and red spots refer to the two domains generated by modulation. Black cross represent systematic absence for the sum of vectors q_{1LTO} and q_{2LTO}' or the sum of q_{1LTO}' and q_{2LTO}.

dx.doi.org/10.1021/ic301165a | *Inorg. Chem.* 2012, 51, 9789−9798

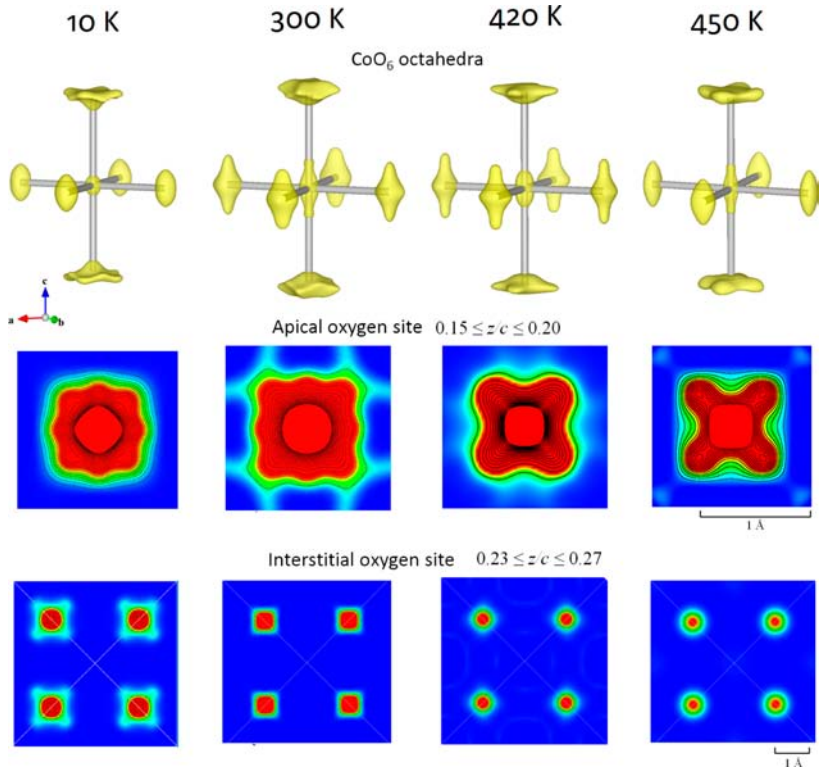

Figure 8. Top part: 3D nuclear intensity profiles of CoO_6 octahedra calculated by Maximum Entropy Method (MEM) using single-crystal neutron diffraction data (main reflections only). Middle part: 2D maps for apical oxygen. Bottom part: 2D maps for interstitial oxygen.

superspace group approach is mandatory for elucidating the real structure in terms of atomic modulation functions. This complex work is currently under progress.

To sum up, the *as-grown* $La_2CoO_{4+\delta}$ compound with $\delta = 0.14$ undergoes a first transition at 413 K from a (3 + 2)D incommensurately modulated orthorhombic structure to a (3 + 1)D incommensurately modulated less orthorhombic one (HTLO), and a second transition at 433 K to a nonmodulated tetragonal structure (HTT).

Neutron Diffraction. A full set of 112 unique main reflections has been measured on a $La_2CoO_{4.14}$ single-crystal of millimetric size ($3 \times 3 \times 5$ mm^3) at 10 K, RT, 420 K, and 450 K. For each data set, the structure has been refined in the average *F*4/*mmm* space group. The symmetry of the basic unit cell remains orthorhombic down to 10 K instead of undergoing a transition toward the Low Temperature Tetragonal (LTT) phase at 103 K, as reported by Gardner et al.[26] for $La_2CoO_{4.15}$.

The choice of a tetragonal space group (average symmetry) even for the orthorhombic modulated phases (below 433 K) has been necessary since the overlapping at low angles of the main reflections of the different domains prevents their separate integration. Consequently, both twinned domains have been averaged in a pseudotetragonal unit cell (space group *F*4/*mmm*). The occupancy of the interstitial oxygen site was refined to the value $\delta = 0.140(2)$. A split model was used for the apical site: in addition to the (0, 0, *z*) position, a second one has been added at the position (*x*, *x*, *z*) sharing the total occupancy of the site to take into account the remaining tilt of octahedra in the average model. The resulting structural model was in better accordance with the experimental data when the supplementary position is partially occupied (from 17% to 30% depending on the temperature), meaning that a percentage of octahedra are not aligned with the *c*-axis, but remain tilted, even in the HTT phase. This tilt can reasonably be attributed to the partial occupancy of O_{int}, which imposes a symmetrical enlargement of O_{int}-O_{ap} tetrahedra causing a rearrangement of tilts between two alternative CoO_6 layers. According to the refinement results, for $\delta = 0.140(2)$ the tilt of octahedra is of about 15° from the *c*-axis corresponding to a O_{ap}-O_{int} bond distances of 2.680(3) Å.

Nuclear densities have been reconstructed by the Maximum Entropy Method (MEM) from phased structure factors using the models given in Table 1. Only main reflections have been used, even for the orthorhombic phases (i.e., excluding satellites). Thus, the reconstructed nuclear densities include the projection of the atomic modulations, and also the twinning is averaged out by combining the contribution of both twin domains. Figure 8 presents the three-dimensional isosurfaces of the nuclear densities corresponding to CoO_6 octahedra for 10 K, RT, 420 K, and 450 K, accompanied with the projections on the *a*-*b* plane of the apical and interstitial sites.

At 10 K, namely, in the LTO phase, the shape of the density for O_{ap} is very complex. With regard to the centroid of density, two main displacements are clearly visible: along the {110} and {100} axes with similar amplitude and probability. The two displacements differ in direction on their *c*-axis component: the {110} one points upward while the {100} one points downward. At RT, a new {110}-displacement appears with another *c*-component, that is, toward the La atom. It is worth stressing that the evolution from 10 K to RT is only due to dynamical effects as no structural phase transition has been detected in this temperature range for the investigated sample.

For HTLO phase, we can appreciate a loss of structuring for the shape of O_{ap}. Moreover the displacements along {100} have vanished. Finally, at 450 K, for O_{ap} only the displacements along {110} pointing slightly toward La are present. In the

dx.doi.org/10.1021/ic301165a | *Inorg. Chem.* 2012, 51, 9789−9798

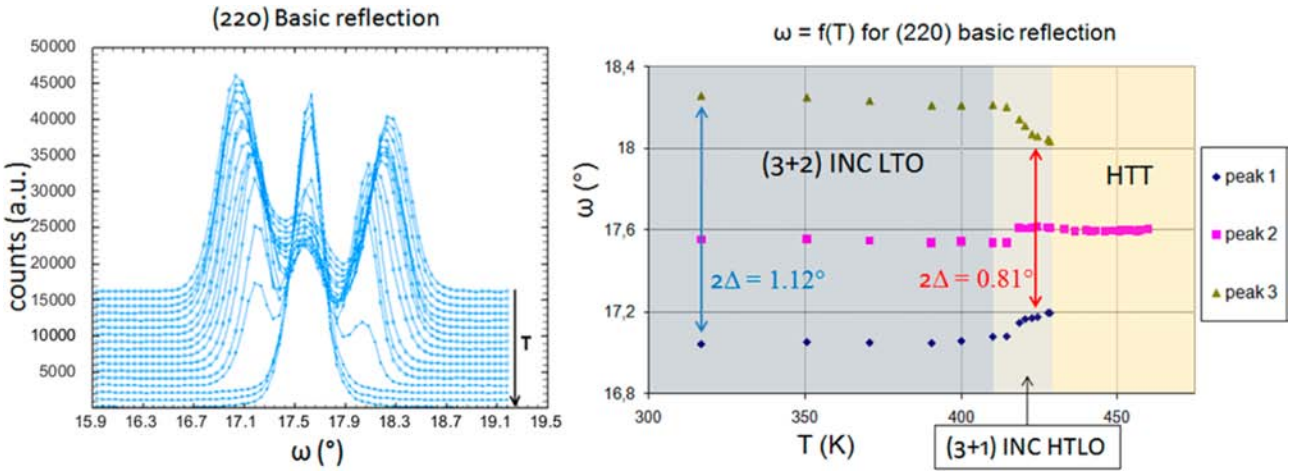

Figure 9. Part (a), ω-scans of 220 reflections as a function of temperature in the range from 380 to 426 K by neutron diffraction (TriCS@SINQ). Part (b), evolution of peaks' position.

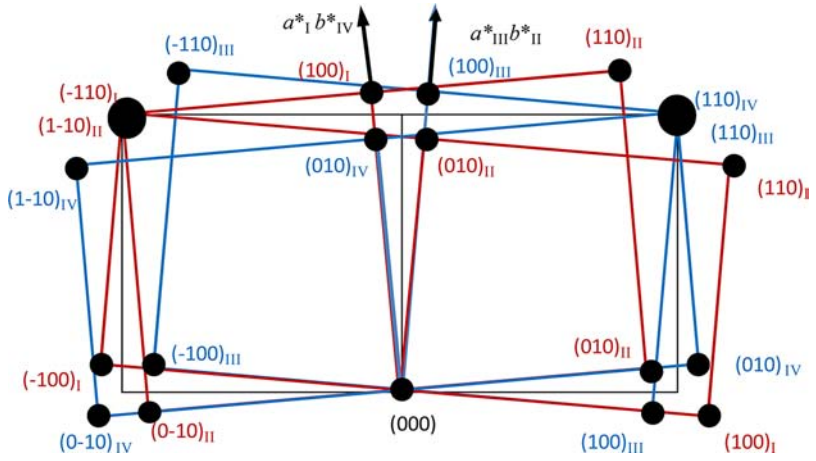

Figure 10. Twin law for sample twice pseudomerohedrally twinned. Averaged tetragonal cell (black full curve), domain I and II (red full curve), and domain III and IV (blue full curve) are represented.

HTT phase O_{ap} is clearly dynamically delocalized over four sites surrounding the most occupied central site of higher symmetry. The lattice site occupied by equatorial oxygen follows the tendency of the Co site to be elongated toward the *c*-axis. This is consistent with a tilt of octahedra which imply not only a shift of O_{ap} but also the corresponding displacement of O_{eq}.

The centroid of O_{int} nuclear density has been found to be located exactly at the ($^1/_4$ $^1/_4$ $^1/_4$) position for all temperatures in agreement with the structural refinements, but an intriguing evolution with temperature can be noticed (Figure 8, bottom part). This atom appears indeed more localized at 450 and 420 K than at RT and 10 K although the opposite trend would be intuitively expected. The apparently isotropic delocalization of O_{int} is associated with the octahedral tilting along {100} that is present only in the LTO phase.

A possible explanation of this phenomenon is that interstitial oxygen position is modulated, and the apparent "delocalization" at lower temperature corresponds to averaging oxygen position along the modulation. During cooling, a set of specific reflections, (220), (−220), (006), plus few satellites, has been measured by ω-scan every 2 K from 470 to 370 K and every 10 K from 370 K to RT. The family of (*hhl*) reflections, consisting of a single peak at 470 K in the HTT phase, split into 3 parts below the tetragonal to orthorhombic transition (around 433 K), as visible for the (220) reflection in Figure 9a and Figure 9b. The splitting into three peaks and not into two as for the *as-grown* sample (see Figure 2) is not surprising; indeed the reversibility of the transition does not imply the conservation of the number of twin domains. In fact we observed the appearance of an additional set of two twin domains, that is, four individual orientations of the basic unit cell in total, domain I and II for the first set, and domains III and IV for the second one. In such case the twin law (Figure 10) can be described as the superimposition of two inverted twinning schemes for 2 domains: the first set in red and the second one in blue on the Figure 10. The total twinning scheme results in the superimposition of the overlapped part of one set with the split part of the other.[40] Consequently, the three peaks shown in Figure 9a could be ascribed to domain I, the sum of domains III and IV, and domain II from left to the right, respectively.

According to the twin law, it has been possible to attribute the following relative amount to each domain with respect to the total volume: I: 10% - II: 14% for the first set, and III: 30% - IV: 46% for the second set. The 00*l*-type reflection only a slight shift during cooling and a minor variation of integrated intensity could be detected. This behavior is expected since the (00*l*) reflections are unaffected by twinning.

dx.doi.org/10.1021/ic301165a | *Inorg. Chem.* 2012, 51, 9789−9798

DISCUSSION

At high temperatures, the stoichiometric compounds $La_2MO_{4.00}$ (M = Co, Ni, Cu) have the ideal K_2NiF_4-type structure denoted as the high temperature tetragonal phase (HTT).[25] In this phase, the space group is *I*4/*mmm* (equivalent to *F*4/*mmm* by a change of unit-cell) and the principal axes of the MO_6 octahedra are aligned along the crystallographic axes. On cooling, the structure undergoes a phase transition to a low temperature orthorhombic phase (LTO) caused by a cooperative tilt of the MO_6 octahedra from the *c*-axis.[6,14,26] For Cu and Ni compounds, this tetragonal to orthorhombic transition has been described in terms of a displacive phase transition induced by a softening of a transverse-optic-phonon mode at the X-point of the Brillouin zone of the *I*4/*mmm* HTT unit cell.[27−29] For La_2NiO_4, the soft phonon mode (1.6 THz) has been attributed to the coherent tilting of the rigid NiO_6 octahedra.[27] The freezing of this specific mode at the transition results in the ordered and static tilting scheme of NiO_6 at RT in the direction $[110]_{HTT}$. The resulting octahedra arrangement implies a doubling of the unit cell ($a\sqrt{2}$, $a\sqrt{2}$, *c*, *F*-centered unit cell) testified by the appearance of superstructure reflections indexed within the *Bmab* space group. The three isostructural systems $La_2MO_{4.00}$ (with M = Co, Ni and Cu) are stable in the LTO phase at RT.

Intercalation of oxygen to form $La_2MO_{4+\delta}$ with $\delta \neq 0$ has two main effects on the local structure: (i) the repulsive interaction between the O_{ap} and O_{int} anions modifies the nearby octahedra arrangement by shifting the surrounding apical oxygen ions from their original position; (ii) the oxidation of two M cations from valence II into valence III for each interstitial oxygen atom, with a consequent reduction of their coordination spheres, induces disparities in the M-O interatomic bond lengths. Because of these local effects, if the concentration of interstitial oxygen ions is sufficient to alter the coherency of tilts of MO_6 octahedra, superstructure reflections belonging to *Bmab* symmetry vanish even if the unit cell remains orthorhombic.[2,9,30] In this situation, the structure can be described with *Fmmm* space group in the LTO unit cell. However the structure described above is only a pictorial view of more complex orders.

This diffraction study has revealed the presence of satellite reflections in the different low temperature phases of $La_2CoO_{4.14}$. Those supplementary reflections arise from additional modulation in the structure, not taken into account by the classic space groups. These complex structural modulations for the Ruddlesden−Popper phases have been already observed for layered cuprates,[31−33] nickelates,[34−37] and cobaltates.[38−41]

The transition at 413 K was unexpected with the loss of modulation along the *c* direction (vanishing of q_{2LTO}), accompanied by the shift of vector q_{1LTO} and an abrupt decrease of orthorhombicity. The existence of an HTLO phase between the HTT and LTO has been never detected for other Ruddlesden−Popper phases, although the phase diagram has been extensively investigated. As previously reported for isostructural compounds, the shift of q_{1LTO} toward q_{1HTLO} can be correlated to the modification of the tilt direction of octahedra. The smaller the angle is between the modulation vector and the *b*-axis, the higher is the orthorhombicity (for δ = 0, q // b and 2Δ is maximum).

The transition from the LTO to HTLO phase is analogous to the transition from LTO to LTLO phase reported in the literature for the family of pure and mixed $Ln_2NiO_{4+\delta}$ (*Ln* = Lanthanide).[42] Indeed in both cases the propagation vector has the tendency to align toward the [110] direction with respect to the *F*-centered unit cell while orthorhombicity decreases. However, the $La_2NiO_{4+\delta}$ LTLO space group is *Pccn* which is not the case here: there are no symmetry modifications in the basic unit cell at 413 K, but a change of long-range modulated ordering.

The transition from HTLO to HTT above 433 K testifies a complete loss of long-range order responsible for satellite reflections. Even if the symmetry changing from *Fmmm* to a higher symmetrical *F*4/*mmm* space group could be assigned to alignment of octahedra with the *c*-axis, it is more reasonable to ascribe it to the loss of coherency in the tilting arrangement. However, considering that the X-ray atomic scattering factor is proportional to the atomic number, it is mandatory to underline that X-ray diffraction is mainly sensitive to the heavy atoms, that is, La in our case. The relatively high intensity of satellite peaks cannot be explained just by the modulation of oxygen positions and occupancies, the structural modulation must involve also La atoms. La positions are obviously correlated to the rest of the structure and their shift from original position strongly depends on the shifts of neighboring atoms. Occupational modulation of interstitial site induces a simultaneous positional modulation of the rest of the structure, which is thus distorted in comparison with the stoichiometric phase.

CONCLUSION

A detailed in situ combined synchrotron radiation and neutron diffraction study on single-crystal has allowed to gain new insights in the thermal phase diagram of as-grown $La_2CoO_{4.14}$. Below 413 K, the crystal structure is very complex because of the presence of multiple twinning effects. In such LTO phase, each domain is (3 + 2)D incommensurately modulated with a bidimensional character ($q_{1LTO} = 0.85a^* + 0.53b^*$ and $q_{2LTO} = -0.23a^* + 0.27b^* + {}^1/_2c^*$). At 413 K, a phase transition occurs toward a HTLO phase that is (3 + 1)D incommensurately modulated ($q_{1HTLO} = 0.783a^* + 0.55b^*$), also accompanied by a strong lowering of orthorhombicity. Upon further heating, above 433 K, the HTLO phase transforms into the so-called HTT phase with concomitant disappearance of satellites, along with orthorhombicity and twinning. It is worth stressing that for the oxides with the K_2NiF_4 structure-type it is the first time that an intermediate phase between the LTO and HTT phase is evidenced. The driving force of both phase transitions could be ascribed to the tilting scheme of the CoO_6 octahedra connected with the ordered pattern of the interstitial oxygen atoms, as suggested by Le Toquin et al.[14] As a matter of fact the nonmodulated HTT phase appears as strongly dynamically disordered because of the tendency of the octahedra to tilt along four directions, as seen in reconstructions of nuclear density by the MEM.

The well-attested displacive interpretation of the HTT to LTO phase transition in terms of TO-phonon mode softening at the X-point of the Brillouin zone (*I*4/*mmm* unit cell) for $La_2NiO_{4+\delta}$ and $La_2CuO_{4+\delta}$ is no longer valid for $La_2CoO_{4.14}$ as it cannot explain by itself the appearance of the q_{1HTLO} modulation. Moreover, we tentatively associate, by the use of the MEM, the tilting of CoO_6 octahedra along {110} directions to vectors q_{1LTO} and q_{1HTLO}, and the tilting along {100} to vector q_{2LTO}. The unexpected isotropic delocalization of O_{int} in the LTO phase may be correlated to the modulation vector

dx.doi.org/10.1021/ic301165a | Inorg. Chem. 2012, 51, 9789−9798

q_{2LTO}. We would like to underline that a correct description of interstitial oxygen ordering and the connected octahedral tilting schemes in terms of modulation is fundamental for a general understanding of oxygen migration in solids as recently highlighted by Kushima et al.[43]

■ ASSOCIATED CONTENT

Supporting Information

Further details are given in Figures S1−S4. This material is available free of charge via the Internet at http://pubs.acs.org.

■ AUTHOR INFORMATION

Corresponding Author

*E-mail: carmelo.prestipino@univ-rennes1.fr (C.P.), werner.paulus@um2.fr (W.P.).

Notes

The authors declare no competing financial interest.

■ ACKNOWLEDGMENTS

We acknowledge the financial support of CNRS and Entwicklungsfonds Seltene Metalle (ESM), Pully, Switzerland, for one of the authors (L.L.D.). This work is based on experiments performed at the Swiss spallation neutron source SINQ (TriCS), Paul Scherrer Institute, Villigen, Switzerland, and at European Synchrotron Radiation Facility ESRF (ID11), Grenoble, France. We would like to thank the "Centre de diffractométrie X" of ISCR (UMR 6226, Rennes) for the preliminary laboratory X-ray data collections. We gratefully acknowledge Jonathan Wright for the support during and after the experiment at ESRF, and Lukas Palatinus (ASCR, Praha, Czech Republic) for a careful rereading of the manuscript as well as fruitful and enlightening discussions.

■ REFERENCES

(1) Bednorz, J. G.; Müller, K. A. *Z. Phys. B: Condens. Matter* **1986**, *64*, 189−193.

(2) Nemudry, A.; Rudolf, P.; Schöllhorn, R. *Solid State Ionics* **1998**, *109*, 213−222.

(3) Takayama-Muromachi, E.; Sasaki, T.; Matsui, Y. *Phys. C (Amsterdam, Neth.)* **1993**, *207*, 97−101.

(4) Blakeslee, P.; Birgeneau, R. J.; Chou, F. C.; Christianson, R.; Kastner, M. A.; Lee, Y. S.; Wells, B. O. *Phys. Rev. B* **1998**, *57*, 13915−13921.

(5) Casañ-Pastor, N.; Gomez-Romero, P.; Fuertes, A.; Navarro, J. M. *Solid State Ionics* **1993**, *63−65*, 938−944.

(6) Grenier, J.-C.; Wattiaux, A.; Lagueyte, N.; Park, J. C.; Marquestaut, E.; Etourneau, J.; Pouchard, M. *Phys. C (Amsterdam, Neth.)* **1991**, *173*, 139−144.

(7) Girgsdies, F. *Solid State Commun.* **1994**, *91*, 111−112.

(8) Radaelli, P. G.; Jorgensen, J. D.; Schultz, A. J.; Hunter, B. A.; Wagner, J. L.; Chou, F. C.; Johnston, D. C. *Phys. Rev. B* **1993**, *48*, 499.

(9) Tamura, H.; Hayashi, A.; Ueda, Y. *Phys. C (Amsterdam, Neth.)* **1993**, *216*, 83−88.

(10) Demourgues, A.; Weill, F.; Darriet, B.; Wattiaux, A.; Grenier, J. C.; Gravereau, P.; Pouchard, M. *J. Solid State Chem.* **1993**, *106*, 330−338.

(11) Yamada, K.; Matsuda, M.; Endoh, Y.; Keimer, B.; Birgeneau, R. J.; Onodera, S.; Mizusaki, J.; Matsuura, T.; Shirane, G. *Phys. Rev. B* **1989**, *39*, 2336.

(12) Kajitani, T.; Hosoya, S.; Hiraga, K.; Fukuda, T. *J. Phys. Soc. Jpn.* **1990**, *59*, 562−570.

(13) Le Toquin, R. Réactivité, structure et propriétés physiques de $SrCo_{2.5+d}$ et LA2CoO$_{4+d}$, étude par diffraction des rayons x et des neutrons in situ. Ph.D. Thesis, Université de Rennes 1, Rennes, France, 2003.

(14) Le Toquin, R.; Paulus, W.; Cousson, A.; Dhalenne, G.; Revcolevschi, A. *Phys. B (Amsterdam, Neth.)* **2004**, *350*, E269−E272.

(15) Oka, K.; Menken, M. J. V.; Tarnawski, Z.; Menovsky, A. A.; Moe, A. M.; Han, T. S.; Unoki, H.; Ito, T.; Ohashi, Y. *J. Cryst. Growth* **1994**, *137*, 479−486.

(16) Lee, C. H.; Kaneko, N.; Hosoya, S.; Kurahashi, K.; Wakimoto, S.; Yamada, K.; Endoh, Y. *Supercond. Sci. Technol.* **1998**, *11*, 891−897.

(17) Labiche, J.-C.; Mathon, O.; Pascarelli, S.; Newton, M. A.; Ferre, G. G.; Curfs, C.; Vaughan, G.; Homs, A.; Carreiras, D. F. *Rev. Sci. Instrum.* **2007**, *78*, 091301.

(18) Petricek, V.; Dusek, M.; Palatinus, L. *Jana2006. The crystallographic computing system*; Institute of Physics: Praha, Czech Republic, 2006.

(19) Schefer, J.; Könnecke, M.; Murasik, A.; Czopnik, A.; Strässle, T.; Keller, P.; Schlumpf, N. *Phys. B (Amsterdam, Neth.)* **2000**, *276−278*, 168−169.

(20) Izumi, F.; Dilanian, R. A. *Transworld Research Network, Trivaladium* **2002**, *3*, 699−726.

(21) Izumi, F.; Kawamura, Y. *Bunseki Kagaku* **2006**, *55*, 391−395.

(22) Momma, K.; Izumi, F. *J. Appl. Crystallogr.* **2011**, *44*, 1272−1276.

(23) Woodward, P. M. *Acta Crystallogr., Sect. B: Struct. Sci.* **1997**, *53*, 32−43.

(24) Smith, M. G.; Manthiram, A.; Zhou, J.; Goodenough, J. B.; Markert, J. T. *Nature* **1991**, *351*, 549−551.

(25) Ganguly, P.; Rao, C. N. R. *J. Solid State Chem.* **1984**, *53*, 193−216.

(26) Paulus, W.; Cousson, A.; Heger, G.; Revcolevschi, A.; Dhalenne, G.; Hosoya, S. *Phys. B (Amsterdam, Neth.)* **1997**, *234−236*, 20−22.

(27) Pintschovius, L.; Bassat, J. M.; Odier, P.; Gervais, F.; Chevrier, G.; Reichardt, W.; Gompf, F. *Phys. Rev. B* **1989**, *40*, 2229.

(28) Birgeneau, R. J.; Chen, C. Y.; Gabbe, D. R.; Jenssen, H. P.; Kastner, M. A.; Peters, C. J.; Picone, P. J.; Thio, T.; Thurston, T. R.; Tuller, H. L.; Axe, J. D.; Böni, P.; Shirane, G. *Phys. Rev. Lett.* **1987**, *59*, 1329.

(29) Böni, P.; Axe, J. D.; Shirane, G.; Birgeneau, R. J.; Gabbe, D. R.; Jenssen, H. P.; Kastner, M. A.; Peters, C. J.; Picone, P. J.; Thurston, T. R. *Phys. Rev. B* **1988**, *38*, 185.

(30) Paulus, W.; Heger, G.; Rudolf, P.; Schöllhorn, R. *Phys. C (Amsterdam, Neth.)* **1994**, *235−240*, 861−862.

(31) Zaanen, J. *Science* **1999**, *286*, 251−252.

(32) Emery, V. J.; Kivelson, S. A.; Zachar, O. *Phys. Rev. B* **1997**, *56*, 6120.

(33) Tranquada, J. M.; Sternlieb, B. J.; Axe, J. D.; Nakamura, Y.; Uchida, S. *Nature* **1995**, *375*, 561−563.

(34) Chen, C. H.; Cheong, S.-W.; Cooper, A. S. *Phys. Rev. Lett.* **1993**, *71*, 2461.

(35) Tranquada, J. M.; Buttrey, D. J.; Sachan, V.; Lorenzo, J. E. *Phys. Rev. Lett.* **1994**, *73*, 1003.

(36) Yamada, K.; Omata, T.; Nakajima, K.; Endoh, Y.; Hosoya, S. *Phys. C (Amsterdam, Neth.)* **1994**, *221*, 355−362.

(37) Tranquada, J. M.; Lorenzo, J. E.; Buttrey, D. J.; Sachan, V. *Phys. Rev. B* **1995**, *52*, 3581.

(38) Zaliznyak, I. A.; Hill, J. P.; Tranquada, J. M.; Erwin, R.; Moritomo, Y. *Phys. Rev. Lett.* **2000**, *85*, 4353−4356.

(39) Horigane, K.; Hiraka, H.; Uchida, T.; Yamada, K.; Akimitsu, J. *J. Phys. Soc. Jpn.* **2007**.

(40) Horigane, K.; Nakao, H.; Kousaka, Y.; Murata, T.; Noda, Y.; Murakami, Y.; Akimitsu, J. *J. Phys. Soc. Jpn.* **2008**, *77*, 044601.

(41) Sakiyama, N.; Zaliznyak, I.; Lee, S.-H.; Mitsui, Y.; Yoshizawa, H. *Phys. Rev. B* **2008**, *78*, 180406R.

(42) Hücker, M.; Chung, K.; Chand, M.; Vogt, T.; Tranquada, J. M.; Buttrey, D. J. *Phys. Rev. B* **2004**, *70*, 064105.

(43) Kushima, A.; Parfitt, D.; Chroneos, A.; Yildiz, B.; Kilner, J. A.; Grimes, R. W. *Phys. Chem. Chem. Phys.* **2011**, *13*, 2242.